Transforming Wave Propagation in Layered Media via Instability-Induced Interfacial Wrinkling

Stephan Rudykh* and Mary C. Boyce†

Department of Mechanical Engineering, Massachusetts Institute of Technology, Cambridge 02139-4307, Massachusetts, USA

(Received 13 September 2013; published 24 January 2014)

The ability to control wave propagation in highly deformable layered media with elastic instability-induced wrinkling of interfacial layers is presented. The onset of a wrinkling instability in initially straight interfacial layers occurs when a critical compressive strain is achieved. Further compression beyond the critical strain leads to an increase in the wrinkle amplitude of the interfacial layer. This, in turn, gives rise to the formation of a system of periodic scatterers, which reflect and interfere with wave propagation. We demonstrate that the topology of wrinkling interfacial layers can be controlled by deformation and used to produce band gaps in wave propagation and, hence, to selectively filter frequencies. Remarkably, the mechanism of frequency filtering is effective even for composites with similar or identical densities, such as polymer-polymer composites. Since the microstructure change is reversible, the mechanism can be used for tuning and controlling wave propagation by deformation.

DOI: 10.1103/PhysRevLett.112.034301 PACS numbers: 43.40.+s, 46.32.+x, 46.40.Cd

Wave propagation phenomena have been investigated intensively because understanding of the phenomena is of great importance for a large variety of applications. Areas of application include nondestructive material testing, acoustic mirrors, waveguides, acoustic filters, vibration dampers, ultrasonic transducers, acoustic and optic cloaking, subwavelength imaging, and photovoltaic devices.

Phononic and photonic metamaterials with periodic microstructures have attracted considerable attention [1–8]. The remarkable properties of the metamaterials originate in their microstructure, a proper choice of which may result in band gaps [1,9–17].

Soft metamaterials, due to their capability to sustain large elastic deformations, open promising opportunities of manipulating wave propagation by deformation. Deformation can influence wave propagation in two ways: first, as a material undergoes large deformation, its microstructure evolves; second, the presence of stress can influence wave propagation. Moreover, the material microstructure (geometry and constituent properties) can be tailored to give rise to elastic instabilities within the internal structure upon achieving critical strain or stress. This phenomenon can be used to trigger sudden and reversible structural pattern transformations [18,19], which can be accompanied by changes in acoustic and optical properties [20–22].

In this Letter, we specifically focus on the influence of instability-induced transformations in interfacial layers on wave propagation in finitely deformed materials. To this end, we consider layered materials with discrete interfacial layers of finite thickness with elastic modulus contrast with the surrounding matrix layers. Upon deformation, the interfacial layer will wrinkle upon reaching a critical compressive strain. The wrinkle takes a sinusoidal waveform with characteristic normalized wavelength $\tilde{l}_{cr}=l_{cr}/h^{(i)}$ can be estimated by $\tilde{l}_{cr}=\pi(((3-4\nu)/(3(1-\nu)^2))((\mu^{(i)})/(\mu^{(m)})))^{1/3}$, where ν is Poisson's ratio, μ is shear modulus, and $h^{(i)}$ denotes interfacial layer thickness [19]. We use the superscripts $()^{(m)}$ and $()^{(i)}$ to denote the quantities associated with matrix and interfacial layers, respectively. The critical strain corresponding to the onset of instabilities is $\epsilon_{cr}=\pi^2(l_{cr}/h^{(i)})^{-2}$.

Examples of the formation of wrinkled interfacial layers are presented in Fig. 1 for composites with $\mu^{(i)}/\mu^{(m)}=100$ and interfacial layer volume fractions of $c^{(i)}=h^{(i)}/h=0.02$ (red) and 0.04 (black). The post-bifurcation behavior is simulated by finite element analysis. The normalized macroscopic stress (left axis) and normalized wrinkled interface amplitude (right axis) $\tilde{A}=A/h^{(i)}$ are given as a function of compressive strain [Fig. 1(c)] . The normalized mean stress is defined via $\tilde{\sigma}=\bar{\sigma}_{11}/\bar{\mu}$, where $\bar{\mu}=c^{(m)}\mu^{(m)}+c^{(i)}\mu^{(i)}$. The dashed curve corresponds to the stress-strain relation for the composite if wrinkling were not to occur. When the compressive deformation is applied, a bifurcation is seen in the stress-strain curve upon reaching the critical strain, which triggers the instability. At this point, a sudden change in microstructure occurs and the wrinkled interfacial layers become visible with the amplitude increasing rapidly with further deformation. Compressive deformation leads to initiation and rapid growth of the amplitude of the wrinkled interface, creating a system of periodic scatterers, which reflect and interfere with propagation of elastic waves. This phenomenon allows control of wave propagation and filtering of particular bands of frequencies by application of deformation.

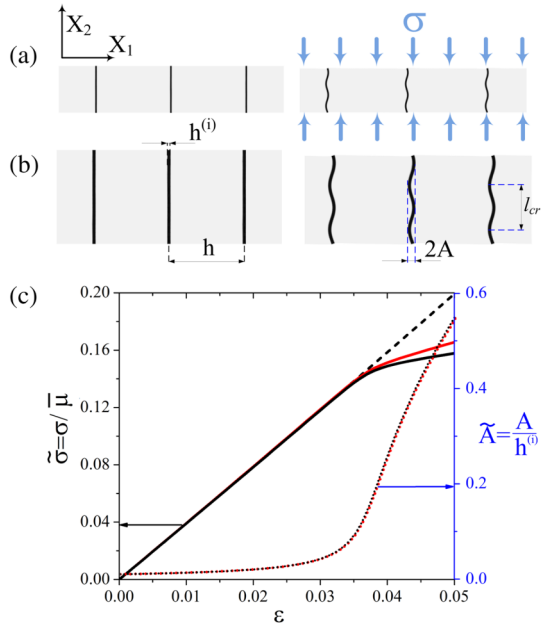

FIG. 1 (color online). Schematics of undeformed and deformed periodic multilayered structures with interfacial phase volume fractions (a) $c^{(i)} = 0.02$ and (b) 0.04. (c) Dependence of stress vs strain and wrinkle amplitude vs strain. The stress-strain results are given by the continuous black ($c^{(i)} = 0.04$) and red curves ($c^{(i)} = 0.02$); the dashed curve is the solution for flat layers, assuming no wrinkling. The dotted curves represent the evolution of the normalized wrinkle amplitude (right axis). The stiffness ratio of the phases is $\mu^{(i)}/\mu^{(m)} = 100$.

Here, we analyze the propagation of elastic waves in finitely deformed periodic materials. To this end, we consider incremental small-amplitude motions superimposed on a finitely deformed state [20]. Differently from a plane wave, a wave propagating in a periodic structure is the superposition of plane waves, which can be described by the Bloch function [1,23]. Consequently, the small-amplitude motions are implemented in terms of Bloch waves $u_i(\mathbf{x}, t) = U_i(\mathbf{x}, t)\exp(i\mathbf{k}\cdot\mathbf{x})$, where u_i is the displacement, $\mathbf{k}$ is the Bloch vector and U_i is a periodic function subjected to the periodicity condition $U_i(\mathbf{x}, t) = U_i(\mathbf{x} + \mathbf{a}, t)$ with $\mathbf{a}$ being a lattice translation vector [12,20,23]. To perform this analysis, we use the finite element method, which allows us (i) to obtain the solution for the deformed periodic composite after the bifurcation, and (ii) then superimpose the Bloch-Floquet periodicity condition on the deformed state and solve the eigenvalue problem associated with the wave equations. For completeness, the numerical solution was verified against exact analytical solutions for finitely deformed infinite homogeneous and layered materials, and excellent agreement was found. We define the direction of wave propagation via angle φ as shown in Fig. 2.

The influence of interface wrinkling on wave propagation is shown in Fig. 3 which compares the dispersion

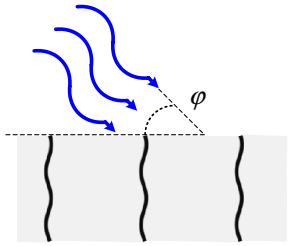

FIG. 2 (color online). Schematics of wave propagation direction with respect to interfacial layers.

diagrams for (a) the undeformed state, where the applied strain $\epsilon = 0$, to (b) those at the onset of wrinkling formation $\epsilon \simeq \epsilon_{cr}$, and to (c) those for a developed wrinkled state $\epsilon > \epsilon_{cr}$. Figure 3 shows examples of dispersion diagrams for various composites with different stiffness ratios $r_\mu = \mu^{(i)}/\mu^{(m)}$: different density contrast ratios $r_\rho = \rho^{(i)}/\rho^{(m)}$, and different interfacial layer volume fractions of $c^{(i)}$ to allow comparison of these effects. The normalized frequency $\tilde{\omega} = \omega h\sqrt{\rho^{(m)}/\bar{\mu}}$ is reported. The dispersion diagram of the undeformed structure appears in the top row. The composites present in columns (1)–(3) and (4) exhibit elastic instabilities at different levels of critical strain, in particular, at $\epsilon^{cr} = 0.040\,08$ and $\epsilon^{cr} = 0.0086$, respectively. Consequently, we present the dispersion diagrams for these cases at different strain levels (middle rows), namely at $\epsilon = 0.04$ for composites in columns (1)–(3) and $\epsilon = 0.01$ for column (4). Finally, we show the dispersion diagrams for a developed wrinkled state in the bottom row for strains of $\epsilon = 0.048$ for composites in columns (1)–(3), and $\epsilon = 0.017$ for column (4). For composites present in columns (1) and (2), the normalized amplitudes of the wrinkles are $\tilde{A} = 0.2687$ and 0.5075 at $\epsilon = 0.04$ and 0.048, respectively. The corresponding amplitudes for the composite (3) are 0.271 and 0.524, respectively. For the composite (4), the amplitudes of the wrinkles are $\tilde{A} = 0.522$ and 1.058 at $\epsilon = 0.01$ and 0.017, respectively.

The dispersion diagrams show different branches of wave propagation including transverse and longitudinal waves. In our analysis, we specifically focus on identifying complete band gaps, when both, longitudinal and transverse waves, cannot propagate. The undeformed composite does not filter waves in a direction along the interface at any frequency; however, the deformed composites with wrinkled interfaces exhibit clear band gaps [see columns (1), (2), and (4) in line (b)]. The frequency range of the band gaps is denoted by the grey filled area in Fig. 3. Note that one-dimensional phononic crystals with flat layers can never prevent wave propagation parallel to the layers [24]. In contrast, the wrinkled interfaces introduce variations of the mechanical properties in the direction of wave propagation, and, consequently, secondary waves are generated. The waves interfere with each other such that for some combination of the material properties,

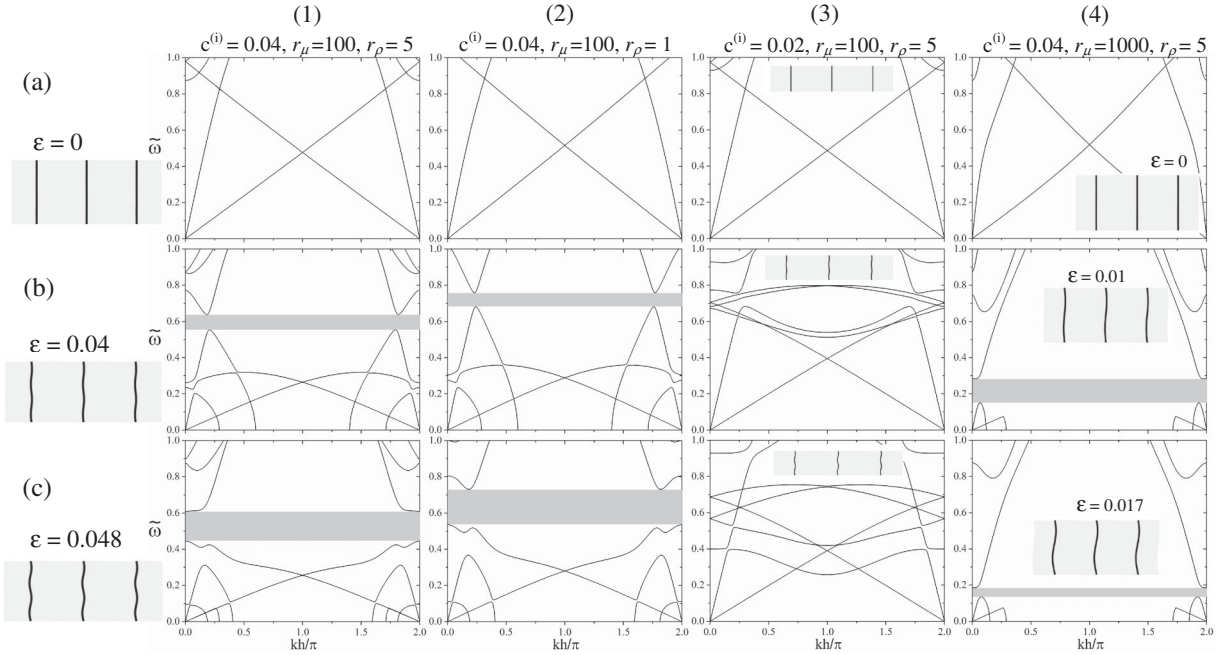

FIG. 3. Dispersion diagrams showing normalized frequency response $\tilde{\omega} = \omega h\sqrt{\rho^{(m)}/\bar{\mu}}$ vs wave number for four composites: $c^{(i)} = 0.04$, $r_\mu = \mu^{(i)}/\mu^{(m)} = 100$ and $r_\rho = \rho^{(i)}/\rho^{(m)} = 5$ [column (1)] and $r_\rho = 1$ (column 2); $c^{(i)} = 0.02$, $r_\mu = 100$ and $r_\rho = 5$ [column (3)]; $c^{(i)} = 0.04$, $r_\mu = 1000$ and $r_\rho = 5$ [column (4)]. The top row is for undeformed states. The middle is for $\epsilon = 0.04$ [columns (1)-(3)] and for $\epsilon = 0.01$ [column (4)]. The bottom row is for $\epsilon = 0.048$ [columns (1)-(3)] and for $\epsilon = 0.017$ [column (4)]. The waves propagate in an initial direction along the interface ($\varphi = \pi/2$).

geometries, wave frequencies, and amplitudes, the reflectance is such that the waves will not propagate. This situation corresponds to band gaps of forbidden frequencies as reported in Fig. 3. We observe no band gaps for the composite with low volume fractions of the interfacial layers [column (3)], even when the wrinkles are well developed. Remarkably, we find that composites with identical densities [column (2)] produce band gaps when the wrinkling interfaces are induced. Finally, for the composites with a higher contrast in the stiffness of the phases, namely $r_\mu = 1000$ [column (4)], we observe that the band gap appeared after wrinkle formation, but the band gap narrowed with further deformation, whereas the band gap broadened for the case with lower stiffness ratio.

The development of band gaps with deformation is shown in Fig. 4 for composites with $c^{(i)} = 0.04$ and $r_\mu = 100$ with density ratios $r_\rho = 1$ (left column) and 5 (right column). Figure 4 shows the evolution of the prohibited frequency ranges as a function of strain for different directions of wave propagation $\varphi = \pi/2$, 0, and $\pi/4$ (from top to bottom). For waves traveling along the layers, $\varphi = \pi/2$, the band gap that appears upon wrinkling initiation shifts to a lower frequency band. The band gap widens due to the evolution in scattering as the wrinkle waveform amplitude and wavelength evolve. There is a change in the band-gap evolution at $\epsilon \simeq 0.045$, when the band gap starts shifting toward higher frequencies. For waves traveling in the direction perpendicular to the layers ($\varphi = 0$) and $r_\rho = 5$, there are two initial band gaps. The first band gap, at higher frequencies, gradually widens with increasing strain. The second band gap, of lower frequencies, rapidly narrows with the deformation until it closes at $\epsilon \simeq 0.005$. This is followed by immediate reopening of the band gap and further widening until $\epsilon \simeq 0.0075$, after which the band-gap width remains constant. For the waves traveling at $\varphi = 0$ in the composite of $r_\rho = 1$, one band gap is observed. The band gap opens at $\epsilon \simeq 0.018$ and then rapidly widens until $\epsilon = 0.021$, after which it continues to widen, although slowly. At $\epsilon \simeq 0.04$, the band gap starts to narrow due to the decrease of the upper boundary, while the lower boundary remains constant. For oblique waves traveling at $\varphi = \pi/4$, the opening and evolution of band gaps are similar to that observed for the case of $\varphi = \pi/2$.

We showed that band gaps can be created in composites with identical densities of the phases when the interfaces take on a wavy topology. The case when both phases have similar densities is of great interest due to the potential for manufacturing light-weight polymer acoustic metamaterials. To highlight the role of the density contrast r_ρ, we present the band gaps as functions of density contrast r_ρ in Fig. 5. The examples are given for composites with $c^{(i)} = 0.04$ and initial stiffness ratios $r_\mu = 100$ (left column) and 1000 (right column). We consider deformation at $\epsilon = 0.048$ (left) and 0.017 (right), where the wrinkled interfaces are developed. The prohibited frequency

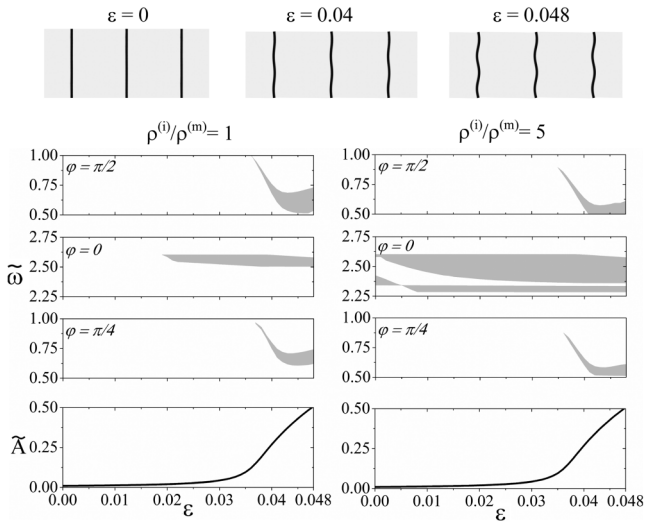

FIG. 4. The prohibited frequency domains and the amplitude of the wrinkled interface as functions of applied strain. The initial stiffness ratio is $r_\mu = 100$, and density contrast ratio is $r_\rho = 1$ (left) and 5 (right). The wave propagation directions are $\varphi = \pi/2$, $\varphi = 0$, and $\varphi = \pi/4$ (from top to bottom).

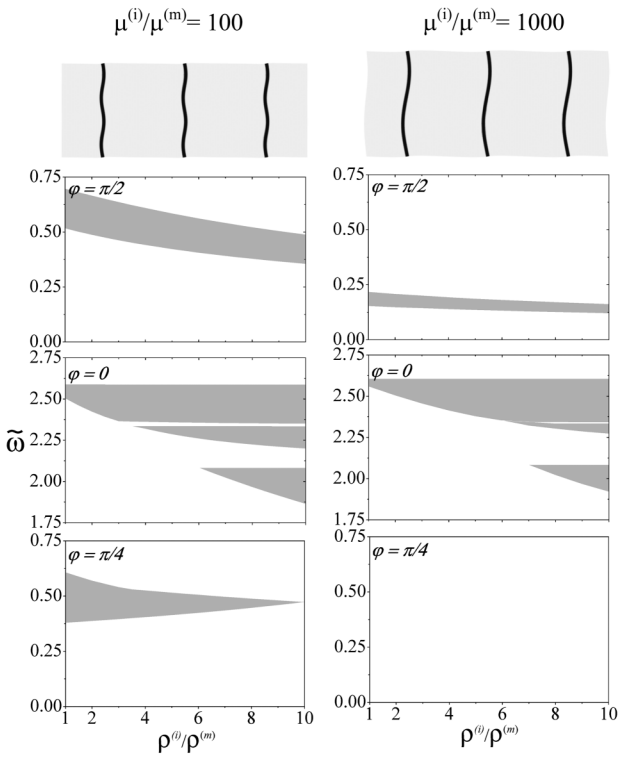

FIG. 5. The prohibited frequency domain as a function of density ratio r_ρ for $r_\mu = 100$ at post-bifurcated state of $\epsilon = 0.045$ (left) and for $r_\mu = 1000$ at $\epsilon = 0.017$ (right) considering interfacial volume fraction of $c^{(i)} = 0.04$. The wave propagation directions are $\varphi = \pi/2$, $\varphi = 0$, and $\varphi = \pi/4$ (from top to bottom).

domains are given for different directions of wave propagation $\varphi = \pi/2$, $\varphi = 0$, and $\varphi = \pi/4$ (from top to bottom). For waves traveling at $\varphi = \pi/2$ in the composite of $r_\mu = 100$, a band gap appears at $r_\rho = 1$. The band gap shifts toward lower frequencies with an increase of r_ρ. For the normal wave propagation ($\varphi = 0$), we observe a rather narrow band gap at $r_\rho = 1$. However, the band gap widens significantly with an increase of r_ρ. Additionally, two new band gaps opens at $r_\rho \simeq 3.6$ and 6, respectively. For oblique waves traveling at $\varphi = \pi/4$, the maximum width of the band gap is reported at $r_\rho = 1$. The band gaps gradually narrow with an increase of r_ρ due to both decreasing of the upper boundary and increasing of the lower boundary. The band gap closes at $r_\rho \simeq 10$.

Composites with the higher stiffness ratio ($r_\mu = 1000$) exhibit a narrow band gap for wave propagation along the layers ($\varphi = \pi/2$). For propagation normal to the interface ($\varphi = 0$), the composite possesses a band gap that broadens with increasing density contrast as well as the emergence of a second band gap when the density ratio exceeds 7. For oblique propagation ($\varphi = \pi/4$), this composite does not have a band gap.

We revealed transformation of wave propagation via instability-induced interfacial wrinkling in composites with interfacial layers. We demonstrated that the formation of the wrinkling interfaces can be used to create band gaps and filter undesirable frequencies. These frequency bands are highly tunable by the material choice and the thickness of layers and the distance between the layers. Since the microstructure change is reversible, the phenomenon is also tunable and reversible depending on the applied stress or deformation. Consequently, we present a novel ability to actively control wave propagation in layered materials. Moreover, this ability applies to material layers with similar or even identical densities of the phases.

Besides the propagation of elastic waves in media with instability-induced interfacial wrinkling, the concept of transforming the wave propagation extends further and can be applied to development of switchable photonic crystals. These optical structures are widely present in nature. However, they are still a challenge to manufacture and are even more challenging to actively control. The study described in this Letter opens up a new prospect for advancing the technology for tunable photonic crystals. The similarities in the phenomena of elastic and electromagnetic (in particular, the optical case) wave propagation, point towards the possibility of extending the idea to switchable photonic crystals. Design of the tunable photonic structures will require additional analyses due to the differences in the phenomena; in particular, elastic waves propagate in longitudinal and transverse modes (these are not pure modes, in general), whereas the polarization of the electromagnetic waves is transverse [25]. Layered materials with varying mechanical and optical phase properties can be manufactured even with ultrathin and subwavelength thicknesses of the layers [26]. Mechanical loadings can be used to induce and control the wrinkling patterns, which may give

rise to a variety of optical effects; for example, silvery iridescence around the eyes of squid (*L. pealeii*) due to the wrinkling pattern of thin layers (80–130 nm [27]) may be mimicked. Moreover, the effect can be further actively controlled by varying the stress or deformation and, as a result, changing the amplitude of the wrinkling interfaces.

This research was supported by the U.S. Army Research Office through the MIT Institute for Soldier Nanotechnologies under Contract No. W911NF-13-D-0001.

*Corresponding author.
rudykh@mit.edu
†Present address: School of Engineering and Applied Science, Columbia University, New York, New York 10025, USA.

[1] M. S. Kushwaha, P. Halevi, L. Dobrzynski, and B. Djafari-Rouhani, Phys. Rev. Lett. **71**, 2022 (1993).
[2] T. Gorishnyy, C. Ullal, M. Maldovan, G. Fytas, and E. Thomas, Phys. Rev. Lett. **94**, 115501 (2005).
[3] A. Akimov, Y. Tanaka, A. Pevtsov, S. Kaplan, V. Golubev, S. Tamura, D. Yakovlev, and M. Bayer, Phys. Rev. Lett. **101**, 033902 (2008).
[4] X.-F. Li, X. Ni, L. Feng, M.-H. Lu, C. He, and Y.-F. Chen, Phys. Rev. Lett. **106**, 084301 (2011).
[5] S. Zhang, C. Xia, and N. Fang, Phys. Rev. Lett. **106**, 024301 (2011).
[6] C. Genet and T. Ebbesen, Nature (London) **445**, 39 (2007).
[7] S. Zhang, D. Genov, Y. Wang, M. Liu, and X. Zhang, Phys. Rev. Lett. **101**, 047401 (2008).
[8] G. Weick, C. Woollacott, W. Barnes, O. Hess, and E. Mariani, Phys. Rev. Lett. **110**, 106801 (2013).
[9] M. S. Kushwaha, P. Halevi, G. MartÃnez, L. Dobrzynski, and B. Djafari-Rouhani, Phys. Rev. B **49**, 2313 (1994).
[10] A. H. Nayfeh, *Wave Propagation in Layered Anisotropic Media: with Applications to Composites* (Elsevier Science, New York, 1995).
[11] M. Aberg and P. Gudmundson, J. Acoust. Soc. Am. **102**, 2007 (1997).
[12] Y. Tanaka, Y. Tomoyasu, and S.-I. Tamura, Phys. Rev. B **62**, 7387 (2000).
[13] J. O. Vasseur, P. A. Deymier, A. Khelif, P. Lambin, B. Djafari-Rouhani, A. Akjouj, L. Dobrzynski, N. Fettouhi, and J. Zemmouri, Phys. Rev. E **65**, 056608/1 (2002).
[14] O. Sigmund and J. Jensen, Phil. Trans. R. Soc. A **361**, 1001 (2003).
[15] H. Zhao, Y. Liu, G. Wang, J. Wen, D. Yu, X. Han, and X. Wen, Phys. Rev. B **72**, 012301 (2005).
[16] M. Gei, Eur. J. Mech. A. Solids **27**, 328 (2008).
[17] L. Hu, L. Liu, and K. Bhattacharya, J. Elast. **107**, 65 (2012).
[18] T. Mullin, S. Deschanel, K. Bertoldi, and M. C. Boyce, Phys. Rev. Lett. **99**, 084301 (2007).
[19] Y. Li, N. Kaynia, S. Rudykh, and M. C. Boyce, Adv. Eng. Mater. **15**, 921 (2013).
[20] K. Bertoldi and M. C. Boyce, Phys. Rev. B **78**, 184107 (2008).
[21] J.-H. Jang, C. Y. Koh, K. Bertoldi, M. C. Boyce, and E. L. Thomas, Nano Lett. **9**, 2113 (2009).
[22] L. Wang and K. Bertoldi, Int. J. Solids Struct. **49**, 2881 (2012).
[23] C. Kittel, *Introduction to Solid State Physics* (Wiley, New York, 2004), 8th ed..
[24] M. Maldovan and E. L. Thomas, *Periodic Materials and Interference Lithography: for Photonics, Phononics and Mechanics* (Wiley-VCH, Weinheim, 2009).
[25] E. G. Henneke and R. E. Green, J. Acoust. Soc. Am. **45**, 1367 (1969).
[26] M. Kats, S. Byrnes, R. Blanchard, M. Kolle, P. Genevet, J. Aizenberg, and F. Capasso, Appl. Phys. Lett. **103**, 101104 (2013).
[27] L. Mathger, E. Denton, N. Marshall, and R. Hanlon, J. R. Soc. Interface **6**, S149 (2009).